RESEARCH ARTICLE
doi: 10.2306/scienceasia1513-1874.2026.036

ScienceAsia 52 (2): 2026: ID 2026036: **1–12**

Zinc porphyrin photosensitizers incorporated with heavy-atom halogens for *in vitro* photodynamic therapy

Gui-chen Li[a,*], Yan-yan Li[b,c,*], Wen-le Zhang[d], Neng-zhi Jin[e], Xiao-xia Feng[b], Jia-cheng Liu[b,*]

[a] State Key Laboratory of Aridland Crop Science, Gansu Agricultural University, Lanzhou 730070 China
[b] Key Laboratory of Eco-Environment-Related Polymer Materials of Ministry of Education, Key Laboratory of Polymer Materials of Gansu Province, College of Chemistry and Chemical Engineering, Northwest Normal University, Lanzhou 730070 China
[c] Tianzhu No. 1 Middle School, Wuwei 733299 China
[d] China National Petroleum Corporation Tarim Oilfield Branch, Korla 841000 China
[e] Key Laboratory of Advanced Computing, Gansu Computing Center, Lanzhou 730099 China

*Corresponding authors, e-mail: lguchen@163.com, jcliu8@nwnu.edu.cn

Received 8 Dec 2025, Accepted 16 Apr 2026
Available online 5 May 2026

ABSTRACT: In this study, three halogenated porphyrins were synthesized through the incorporation of heavy atoms (F, Cl, and Br). Subsequently, to enhance their solubility and bioavailability, zinc atoms were introduced via N-pyridyl-substituted alkylation. This approach culminated in the development of three water-soluble, zinc-containing porphyrins (ZnP1–ZnP3), which were employed as photosensitizers (PSs) for photodynamic therapy (PDT). Our findings indicate that ZnP1–ZnP3 can consistently generate singlet oxygen ($^1O_2$) at concentrations significantly higher than that of the reference compound, tetraphenylporphyrin (TPP), under light irradiation at wavelengths of 600–610 nm. This result is in concordance with the outcomes of the 3-(4,5-dimethylthiazol-2-yl)-2,5-diphenyltetrazolium bromide (MTT) assay, and the cytotoxicity profile reveals that the inhibition rate of human umbilical vein endothelial cells (HUVECs) is virtually negligible. Furthermore, cell staining or cycle analysis, and Reactive Oxygen Species (ROS) detection experiments collectively demonstrate that light-activated PSs can induce apoptosis in cancer cells and produce ROS, which are instrumental in the eradication of these cells. Under dark conditions, these complexes exhibit negligible cytotoxicity. In contrast, they reliably produce $^1O_2$ under light irradiation. Furthermore, due to the heavy atom effect, bromine-containing ZnP3 achieves the highest *in vitro* photocytotoxic efficacy among the three photosensitizers.

KEYWORDS: water-soluble, zinc porphyrins, singlet oxygen, photosensitizers, photodynamic therapy

INTRODUCTION

Cancer has emerged as the preeminent cause of death worldwide, primarily attributed to its propensity for metastasis, robust metabolic capacity, and rapid cell proliferation [1–3]. Characterized by uncontrolled cell growth, cancer affects not only the blood system but also results in the formation of abnormal cell clusters or tumors in various tissues. Given these challenges, the development of effective cancer treatments is of paramount importance. Presently, the most commonly employed cancer treatments include surgical therapy, chemotherapy, and radiation therapy [4]. However, these conventional methods are often associated with significant side effects and limitations. In light of these issues, photodynamic therapy has garnered considerable attention as a non-invasive alternative for treating specific tissues [5]. PDT comprises three essential components: a photosensitizer, a light source, and molecular oxygen. During PDT, the photosensitizer introduced into the body is activated from its ground state (S0) to the singlet state (S1) upon illumination. It then transitions to the triplet state (T1) via intersystem crossing, where it interacts with surrounding oxygen molecules to generate reactive oxygen species, particularly singlet oxygen [6]. This process is crucial, as these ROS, especially singlet oxygen, oxidize vital cellular macromolecules, leading to the selective destruction of tumor cells while sparing unaffected normal cells [7]. Importantly, the PSs remain inert in the dark and does not generate ROS or exhibit pharmacological activity. Moreover, the unique properties of ROS contribute to the precision of PDT. Reactive oxygen species react only within 100–150 nm ($^1O_2$, $\sim 3\ \mu s$; $\bullet O_2^-$, $\sim 1\ \mu s$; $\bullet OH$, < 100 ns), so their oxidative effects on DNA, proteins, and lipids are confined to the immediate nanoscale vicinity, limiting tumor-cell kill beyond that range [8, 9]. Given the high reactivity and brief lifespan of ROS, PDT exerts its therapeutic effect only in the immediate vicinity of the PS location. This localized action leads to the breakdown of the target tissue, thereby effectively eradicating the lesion without widespread damage to healthy tissue [10].

Photodynamic agents play a pivotal role in photodynamic therapy, and the selection of PSs is a key determinant of PDT efficacy. Since the pioneering application of hematoporphyrin derivative (HpD) for tumor treatment, porphyrins and their derivatives have attracted considerable attention as PSs for PDT. However, several intrinsic limitations, including pronounced self-aggregation, inadequate aqueous solubility, and lack of tumor specificity, have collectively contributed to suboptimal PDT outcomes [11]. Given these challenges, the identification of novel PSs with enhanced aqueous solubility, minimal dark toxicity, superior plasma membrane permeability, robust singlet oxygen generation, and the ability to selectively engage with specific cellular targets remains a significant pursuit. Most biological systems exist in aqueous environments, yet many synthetic porphyrins and their derivatives exhibit either poor water solubility or insolubility. These properties often result in inefficient targeting of malignant tissues and pronounced aggregation in aqueous media [12]. Consequently, the development and synthesis of water-soluble porphyrin compounds as PSs for PDT are of critical importance. Enhancing the hydrophilicity of PDT agents can significantly improve their circulation and distribution within the bloodstream. This objective can be achieved through chemical modifications such as sulfonation, carboxylation, or alkylation of N-pyridyl-substituted compounds.

The heavy atom phenomenon is essential for the generation of $^1O_2$ during photodynamic therapy. Heavy atoms enhance spin-orbit coupling (SoC), thereby increasing the intersystem crossing (ISC) rate and singlet oxygen quantum yields in photosensitizers [13–15]. This enhancement, commonly referred to as the heavy atom effect, significantly impacts PDT efficacy. Specifically, the incorporation of halogen atoms augments the spin-orbit matrix elements, with the SoC value increasing as the atomic size of the halogen atom increases from fluorine to bromine. Given these findings, the integration of halogen atoms is frequently employed for efficient triplet sensitization and the development of effective photosensitizer molecules. Consequently, the utilization of halogen atom in photosensitizers for PDT is crucial to meet the treatment needs and characteristics.

Metallization has been recognized as a promising strategy for modulating the photophysical properties of photosensitizers in phototherapy [15]. This approach can modify the electrochemical, photochemical, and photophysical characteristics of PSs, thereby enhancing their therapeutic efficacy [13]. Porphyrins and their derivatives are capable of chelating a broad spectrum of metal ions, including Mg, Al, Mn, Fe, Pt, and Lu [16]. This chelation is facilitated by the unique delocalized π-electrons within their rigid frameworks. Specifically, the coordination of zinc with the porphyrin ring reduces hydrophobicity and augments cellular uptake of the PSs. Given these advantages, metallization offers significant benefits for many tetrapyrrole-based photosensitizers. Moreover, the hydrophilicity and specific retention of PSs in malignant tumors are critical factors for their successful application as photodynamic therapy agents [17].

In accordance with the aforementioned findings, we synthesized three halogenated porphyrins by incorporating halogen atoms (F, Cl, and Br). Utilizing this porphyrin framework, zinc was introduced via N-pyridyl-substituted alkylation, which enhanced the solubility and biocompatibility of the resulting compounds. Consequently, three zinc-containing complexes (ZnP1, ZnP2, and ZnP3) were successfully obtained. Given that the atomic radius increases from fluorine to bromine, the ΔE value (HOMO-LUMO energy gap) of the photosensitizer containing bromine is lower than that of its fluorine- and chlorine-containing counterparts. As a result, the bromine-containing photosensitizer demonstrates superior singlet oxygen generation and a more potent cancer cell inhibition effect. These findings underscore the significance of the zinc porphyrin structure. The selection of zinc porphyrin was motivated by the versatility of the metal porphyrin photocenter, which allows for extensive peripheral chemical modification while retaining the essential photochemical activity of the parent compound.

MATERIALS AND METHODS

Synthesis of water-soluble zinc porphyrins ZnP1-ZnP3

Step 1. Synthesis of halogenated ligands

4-Pyridinecarboxaldehyde (2.13 ml) and the corresponding *p*-halobenzaldehyde (1.43 ml) were dissolved in propionic acid (160 ml) and heated to 120 °C. Freshly distilled pyrrole (2.6 ml) was added dropwise, and the reaction mixture was maintained at 140 °C for 90 min. After cooling to room temperature, the solvent was removed in vacuo. The residue was triturated with methanol (150 ml), stirred for 30 min, and stored at 4 °C overnight. The precipitate was collected by filtration and purified by silica gel column chromatography to afford ligands L1 (X = F), L2 (X = Cl), and L3 (X = Br) in 3.5% isolated yields.

Step 2. Zinc insertion

Ligand L1 (50 mg) was dissolved in CH_2Cl_2/CH_3OH (4:1, 50 ml) and treated with $Zn(CH_3COO)_2 \cdot 2\,H_2O$ (200 mg). The mixture was stirred at 50 °C for 5 h, concentrated, and extracted with CH_2Cl_2/H_2O. The resulting purple solid was purified by column chromatography to afford ZnL1 in a 95% yield. The same procedure was applied to L2 and L3 to yield ZnL2 and ZnL3, respectively.

Step 3. N-pyridinium alkylation (water solubilization)

ZnL1 (100 mg) was dissolved in anhydrous DMF (3 ml) and treated with excess CH_3I. The mixture was stirred at 50 °C for 3 h in the dark. CH_2Cl_2 was added to precipitate the product, which was collected by filtration, washed with CH_2Cl_2, and dried to afford the target photosensitizer ZnP1. ZnP2 and ZnP3 were obtained analogously from ZnL2 and ZnL3.

Accurately weighed samples of the products and benzoic acid (99.5% purity) were dissolved in DMSO-d_6 (450 µl) in 5 mm NMR tubes. Purity was determined by quantitative NMR [18] using benzoic acid as internal standard (reference peak at 7.5 ppm) by comparing the integral ratio between the porphyrin methyl group peak (4.6 ppm) and the benzoic acid peak. This method was applied to determine the purity of all three compounds. The specific calculation formula is as follows:

$$P_a = \frac{I_a}{I_s} \times \frac{N_s}{N_a} \times \frac{M_a}{M_s} \times \frac{W_s}{W_a} \times P_s$$

P_a and P_s are the purity of the product and benzoic acid, respectively. I_a is the integral area of the methyl group of the porphyrin compound at around 4.6 ppm. I_s is the peak of benzoic acid around 7.5 ppm. N_x is the compound of nuclear numbers. M_x is formula weight. W_x is the compound qualities.

Density functional theory (DFT) calculation

DFT calculations were carried out using Gaussian 16 A03. Geometry optimizations and frequency analyses employed PBE0-D3(BJ)/def2-SVP, while TD-DFT used PBE0/def2-TZVP for C, H, N, F, Cl, Br, I, and Zn atoms. Spin coupling constants were calculated with PySOC.

Excitation light source

LED irradiation was performed using a 600 nm LED array. The irradiation parameters were as follows: total radiant power $\Phi_e = 6.64$ mW, radiant exitance $M_e = 0.200$ mW/cm^2, irradiance at the cell plane $E_e = 0.183$ mW/cm^2, and radiant exposure (fluence) $H_e = 0.110$ J/cm^2, delivered continuously for 10 min. This fluence was selected to lie within the *in vitro* Klein-saturated zone for 600 nm light (0.08–0.15 J/cm^2), thereby optimizing singlet oxygen generation while producing a negligible thermal dose ($\Delta T < 0.3\,°$C). It is also consistent with the lower end of the effective fluence range (0.05–0.20 J/cm^2) commonly reported in cellular PDT studies.

Cell lines and cell culture

Hepatocellular carcinoma-G2 (HepG2) liver cancer cells and Michigan Cancer Foundation-7 (MCF-7) were kindly provided by Gansu Agricultural University (Lanzhou, China). Cells were grown in 75 cm^2 culture flasks as adherent monolayer cultures in complete medium, consisting of Dulbecco's Modified Eagle Medium (DMEM) or Roswell Park Memorial Institute 1640 (RPMI 1640) for HepG2, and containing 10% fetal bovine serum (FBS). Cultures were maintained at 37 °C in a constant atmosphere containing 5% CO_2 in cell incubator.

Cell viability

On a 96-well cell culture plate, HepG2 cells were washed with PBS and divided into two groups (0.5×10^4 cells per well). ZnP1–ZnP3 were diluted in PBS using RPMI 1640 medium to obtain different concentrations (0.2, 0.5, 0.8, 1.0, 1.5, and 2.0 µM), and the resulting solutions were then added to all wells. One group was placed in the dark, and the other group was irradiated with LED light (600–610 nm) for 10 min after 24 h of incubation. The cells were incubated for another 24 h, after which MTT solution (0.5 mg/ml, 20 µl) was added. Following continuous incubation at 37 °C in 5% CO_2 for 4 h, the cells were treated with DMSO (150 µl). The absorbance at 570 nm was measured using a BioTek microplate reader.

In vitro photodynamic therapy

In order to assess the *in vitro* cytotoxicity in cancer cells, HepG2 cells (5×10^4 cells per well) were seeded into confocal culture plates and incubated with ZnP1–ZnP3 at 37 °C for 24 h. The cells were then exposed to LED light (600–610 nm) for 10 min. The circular probe (∅ 3 cm, 7.1 cm^2 area) was positioned 5 cm above the monolayer, yielding a uniform, flat - top beam with < 5% spatial deviation over the 6-well plate. Negative control for cytotoxicity/ROS generation: cancer cells treated with ZnP1–ZnP3 kept in complete darkness during the irradiation period. Light – only control: cells exposed to the 600 nm LED source in the absence of any photosensitizer. After staining with Hoechst 33342 and propidium iodide (PI), the cell condition was observed under a fluorescence microscope. PI was excited at 488 nm, and Hoechst 33342 was excited at 352 nm. The full specifications of the fluorescence microscope are as follows: system name: Revolve RVL-100-G digital fluorescence microscope; manufacturer: Echo Laboratories, Inc., San Diego, CA, USA; software version: Revolve Imaging Software v4.2.0; hardware configuration: Equipped with 4 × /10 × /20 × /40 × objective lenses and an integrated LED light source.

Cell cycle analysis

Cells were suspended at a density of 0.5×10^6 cells in 1 ml of PBS in 5 ml tubes. The cells were centrifuged at $200 \times g$ for 5 min. The cell pellet was resuspended in 500 µl of cold 1 × PBS. While the tube was gently vortexed, 1 ml of ice-cold 70% ethanol (pre-chilled at −20 °C) was slowly added dropwise to the cell suspension. The cells were incubated overnight at −20 °C. The cells were centrifuged at $200 \times g$ for 5 min and then washed once with 500 µl of cold 1 × PBS. The cells were resuspended in 500 µl of PI solution (containing 50 µg/ml propidium iodide and 200 µg/ml RNase in 1 × PBS). The samples were incubated at room temperature for approximately 30 min in the dark. The cells were transferred to a 5 ml polystyrene flow cytometry tube. The samples were kept on ice and transported to the flow cytometer.

The following control conditions were included in the experiment: a negative (untreated) control consisting of cancer cells incubated in complete medium without any photosensitizer and kept in the dark; a light-only control in which cells were exposed to the 600 nm

LED source in the absence of any photosensitizer; an instrument blank using PBS alone to set forward- and side-scatter thresholds; and single-stain controls using PI-only samples for compensation of spectral overlap.

Flow cytometer settings

A BD FACSVersa (BD Biosciences, USA) was used. The 488 nm blue laser with a 610/20 nm band-pass filter (FL2-A) was used for PI detection. More than 20,000 events per sample were acquired at a low flow rate (12 µl/min), and the data were analyzed using FACSuite v1.0 software.

Intracellular ROS detection

The 2′,7′-dichlorofluorescein diacetate (DCFH-DA) dyes were used in the ROS production experiment. HepG2 cells were cultured with ZnP1–ZnP3 solutions at different concentrations (0.5 µM, 2 µM) in a six-well plate with cover glass and incubated at 37 °C in a humidified 5% CO_2 atmosphere for 24 h. Then, the cells were incubated with 10 µM DCFH-DA for another 30 min and irradiated under an LED light for 10 min, and the ROS fluorescence images of the cells were then observed using a fluorescence microscope. Intracellular ROS were visualized using a Revolve RVL-100-G digital fluorescence microscope (Echo Laboratories) running Revolve Imaging Software v4.2.0. Fluorescence was excited using the instrument's built-in 470 nm LED and collected through a 525/50 nm emission filter using a 20 × objective. Images were captured using a 5 MP CMOS camera (12-bit depth) while cells were maintained at 37 °C and 5% CO_2 in a stage-top incubator.

RESULTS AND DISCUSSION

Characterization of porphyrins ZnP1–ZnP3

Fig. 1 depicts the synthesis of the porphyrin photosensitizers ZnP1–ZnP3. Furthermore, the successful synthesis of ZnP1–ZnP3 was confirmed by high-resolution mass spectrometry (HRMS). The structures of these photosensitizers were authenticated using ^{1}H NMR spectroscopy (Fig. S1).

To further validate the structure of the ZnP1–ZnP3 molecules and confirm their successful synthesis, we conducted infrared spectroscopy analysis on the complexes and ligands. As depicted in Fig. 1D, the ligand exhibits two distinct peaks at 3313 cm^{-1} and 968 cm^{-1}, which are attributed to the stretching vibration of the N–H bond on the porphyrin ring and the in-plane bending vibration, respectively. Notably, these peaks are absent in the infrared spectrum of ZnP1. Instead, a unique peak emerges near 997 cm^{-1}, which is attributed to the coordination between the nitrogen atom and zinc within the porphyrin ring [19, 20]. Collectively, these findings provide further evidence supporting the successful synthesis of the complex.

Singlet oxygen generation

1,3-diphenylisobenzofuran (DPBF) was used as a fluorescent probe for the detection of singlet oxygen. DPBF has a strong absorption peak at 415 nm [21]. Photosensitizer irradiation generates singlet oxygen, which oxidizes DPBF to O-benzoylbenzene. O-benzoylbenzene has no ultraviolet absorption at 415 nm [22]. Therefore, the reduction of absorbance of DPBF can be used for the qualitative and quantitative analysis of singlet oxygen. 5,10,15,20-tetraphenylporphyrin (TPP) is a typical hydrophobic photosensitizer with a high triplet quantum yield [23]. Its solution has been used as a standard to compare the performance of other photosensitizers. Here, TPP is taken as the reference to calculate the singlet oxygen yield of the photosensitizer [24].

As illustrated in Fig. 2A, the absorption band of DPBF at 414 nm exhibited a significant decrease, indicating that ZnP1 and ZnP3 can effectively generate singlet oxygen for PDT under light irradiation. The relative efficiency of singlet oxygen production among ZnP1–ZnP3 follows the order: ZnP3 > ZnP2 > ZnP1. This observation suggests that porphyrin compounds containing bromine atoms exhibit a higher capacity for singlet oxygen generation than those containing fluorine and chlorine. In contrast, the UV absorption profile of the complex shows a more rapid decline than that of the ligand, demonstrating that the complex is more efficient in singlet oxygen production. Additionally, the attenuation rate comparison of ZnP1–ZnP3, as shown in Fig. 2B, indicates that ZnP1-ZnP3, which oxidize DPBF, have attenuation rates significantly higher than that of TPP, which does not absorb in the ultraviolet region. To assess the photostability of these compounds, we monitored the decrease in UV absorption intensity at 10 s intervals over various illumination durations. The results reveal that the absorption curves for TPP and DPBF remained largely unchanged, underscoring the excellent photostability of porphyrins and their derivatives (Fig. 2C).

Utilizing TPP as a benchmark ($\Phi\Delta = 0.64$ in DMSO), we employed the established methodology for calculating singlet oxygen quantum yield. The singlet oxygen quantum yields ($\Phi\Delta$) for ZnP1, ZnP2, and ZnP3 were determined to be 0.68, 0.72, and 0.85, respectively (Table 1). These values are considerably higher than those reported for many conventional porphyrin-based photosensitizers. For example, typical water-soluble sulfonated porphyrins such as tetraphenylporphyrin derivatives exhibit $\Phi\Delta \approx 0.80$ in aqueous media [13], while previously reported halogenated zinc porphyrins generally show $\Phi\Delta$ values between 0.70 and 0.95 [25]. Notably, the $\Phi\Delta$ of ZnP3 (0.85) exceeds that of the commonly used reference compound tetraphenylporphyrin and approaches the efficiency of some high-performance heavy-atom-substituted photosensitizers, such as phenalenone

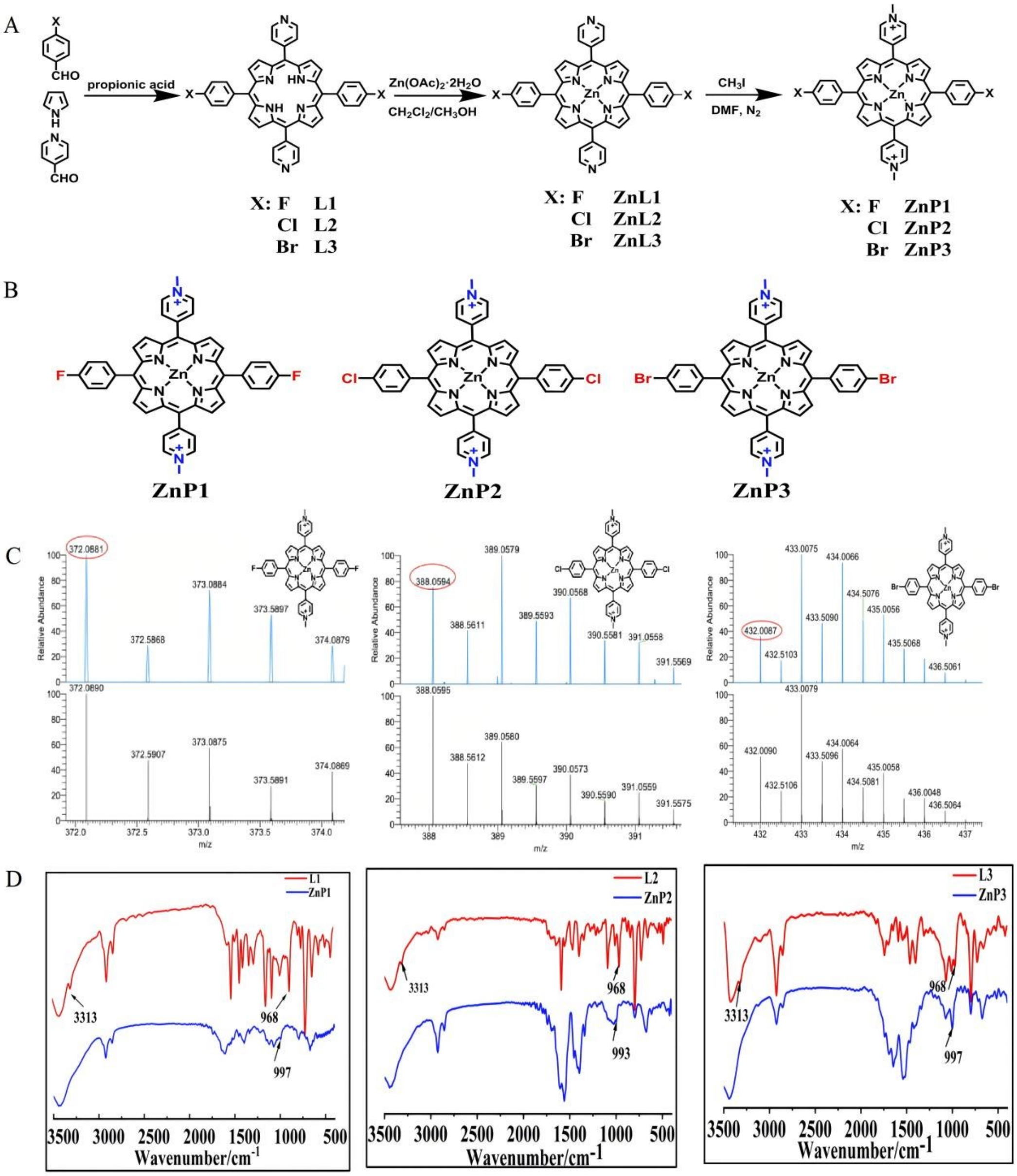

Fig. 1 (A) Synthesis of water-soluble porphyrins ZnP1–ZnP3. (B) Synthesis of ZnP1–ZnP3. (C) HRMS of compounds ZnP1–ZnP3. (D) The FT-IR spectra of L1, L2, L3, ZnP1, ZnP2, and ZnP3.

Table 1 Singlet oxygen and fluorescence quantum yields of ZnP1–ZnP3.

Photosensitizer	$\Phi\Delta$ (singlet oxygen)	Φf (Fluorescence quantum yields)	SOC (cm^{-1})	Halogen substitution	Ref.
ZnP3 (this work)	0.85	0.0756	3903.99	Br	This study
ZnP2 (this work)	0.72	0.1415	1.98	Cl	This study
ZnP1 (this work)	0.68	0.1416	3.31	F	This study
TPP (standard)	0.80	0.11	–	–	[38]
ZnTPPF4	$\ll 1$	–	1.79	F	[22]
ZnTPPCl4	$\ll 1$	–	1.43	Cl	
ZnTPPBr4	< 1	–	21.60	Br	
ZnTPPI8	≈ 1	–	310.03	I	
Phenalenone	≈ 1	< 0.01	–	–	[38]

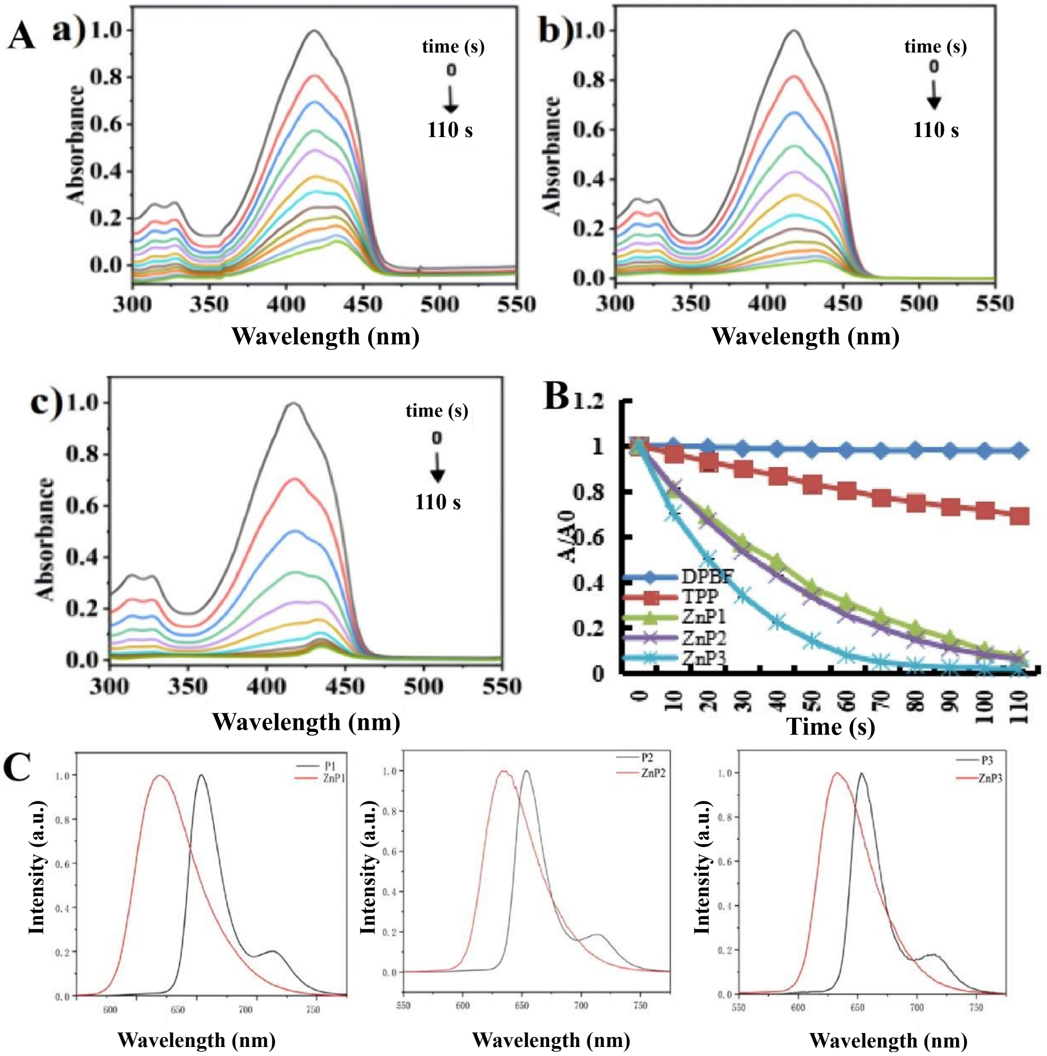

Fig. 2 (A) Time-dependent UV-Vis absorption spectra of DPBF with ZnP1 (a), ZnP2 (b), and ZnP3 (c) in DMSO under 600–610 nm LED irradiation from 0 to 110 s. (B) Comparison of the decay rate of DPBF, TPP, and ZnP1-ZnP3. (C) Fluorescence emission spectra of P1, ZnP1, P2, ZnP2, P3, and ZnP3. Normalized fluorescence intensity (a.u.).

($\Phi\Delta \approx 1.00$ in water) [13]. This enhancement can be attributed to the synergistic combination of zinc metallation and heavy-atom (Br) substitution, which collectively promote intersystem crossing and increase the triplet-state population. Furthermore, Table 1 also includes the fluorescence quantum yield data for these compounds.

Density functional theory (DFT)

The molecular orbital distributions of photosensitizers ZnP1–ZnP3 were plotted with Multiwfn and VMD (Fig. 3) [26, 27]. For all three complexes, the LUMO is delocalized over the inner porphyrin macrocycle and the pyridinium rings, whereas the HOMO resides mainly on the halogen-substituted phenyl segments and the meso-carbon bridges (Fig. 3A). This spatial separation indicates an intra-molecular donor-acceptor character that facilitates excited-state charge transfer. Although the HOMO-LUMO energy gap is almost constant, the singlet-triplet splitting ΔE_{ST} decreases markedly from ZnP1 (0.72 eV) to ZnP3 (0.06 eV) because the heavy-atom substituents differentially stabilize the triplet state (Fig. 3B,C). The smaller ΔE_{ST} and the larger spin-orbit coupling constant (SOC) of ZnP3 (3903.99 cm^{-1}) jointly accelerate intersystem crossing, consistent with its highest singlet-oxygen quantum yield.

Augmenting the intersystem crossing (ISC) between the lowest singlet (S_1) and the lowest triplet (T_1) states enhances the efficacy of photodynamic therapy [28]. Based on the first-order perturbation theory and the Marcus semiclassical approach, two strategies

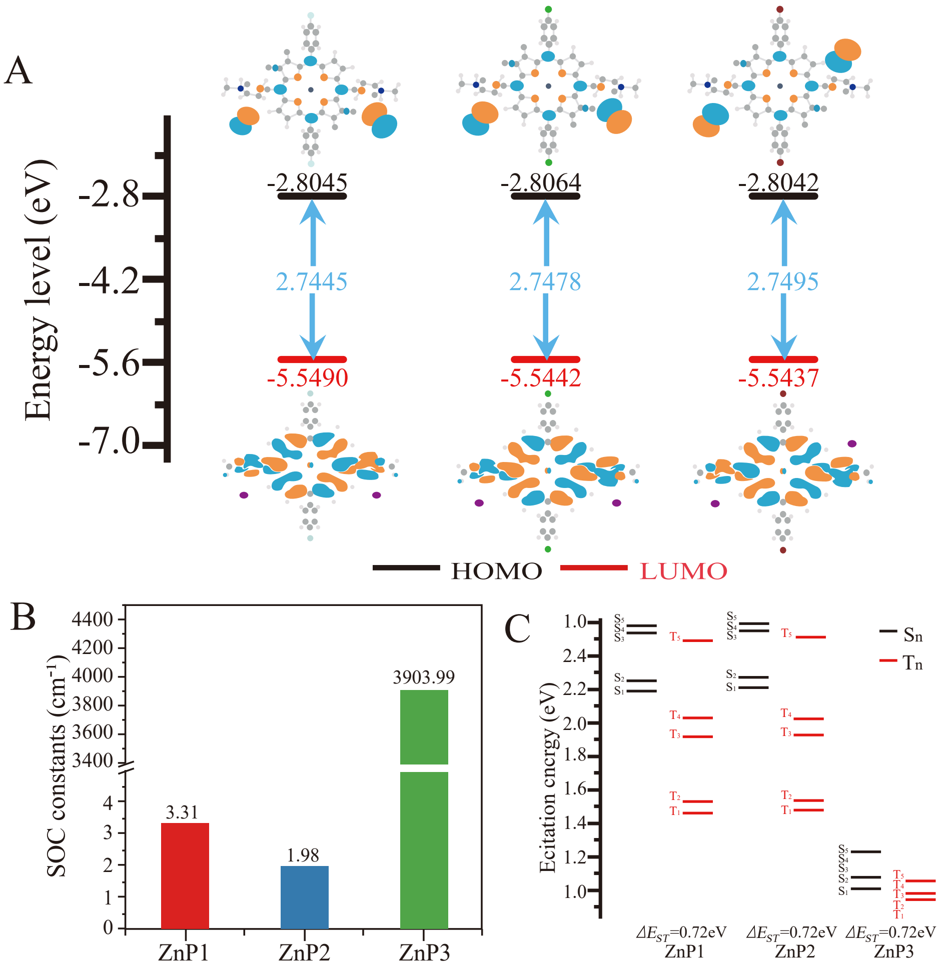

Fig. 3 (A) Molecular frontier orbital amplitude plots of ZnP1, ZnP2, and ZnP3, calculated by PBE0-D3(BJ)/def2-SVP. (B) Spin-orbit coupling constants of ZnP1, ZnP2, and ZnP3. (C) Calculated excitation energy distributions for singlet (S_n) and triplet (T_m) excited states.

have been identified to achieve more efficient ISC: (1) reducing the energy gap (ΔE_{ST}, defined as the energy difference between the lowest singlet excited state S_1 and the lowest triplet excited state T_1, i.e., $\Delta E_{ST} = E(S_1) - E(T_1)$) between S_1 and T_1, and (2) enhancing the SOC process. The rate constant for transitions between these states exhibits a quadratic relationship with the Hamiltonian of SOC, indicating that spin-orbit coupling significantly influences the efficiency of ISC. Given these findings, optimizing the therapeutic impact of ISC on photosensitizers is essential. Consistent with this objective, the literature indicates that narrowing the energy gap (ΔE_{ST}) between the singlet and triplet states increases the transition rate.

Consequently, the ΔE_{ST} and SOC values of the three photosensitizers were determined (Fig. 3B,C) [29]. The results revealed that, despite significant variations in the HOMO-LUMO energy gap values among the three photosensitizers, ZnP3 exhibited a lower singlet-triplet energy gap (ΔE_{ST}) value (0.06 eV) and the highest SOC value (3903.99 cm^{-1}). The SOC constants for the fluorine- and chlorine-substituted analogs (ZnP1 and ZnP2) are exceedingly low (3.31 and 1.98 cm^{-1}), which aligns with the understanding that light halogen atoms (F and Cl) contribute minimally to SOC enhancement [30–32]. The result is in excellent agreement with the established heavy-atom effect [33, 34]. Although absolute values differ, both studies capture the same essential trend: bromine substitution provides a decisive boost in SOC, highlighting its critical role. Based on these findings, theoretical analyses suggest that ZnP3 demonstrates superior efficacy in photodynamic therapy.

Cytotoxicity

To assess the cell compatibility of ZnP1–ZnP3 under dark conditions and their cytotoxicity under light conditions, we employed the MTT assay to evaluate their phototoxicity. We selected two types of cancer cells, HepG2 and MCF-7, and normal cells (HUVEC) to

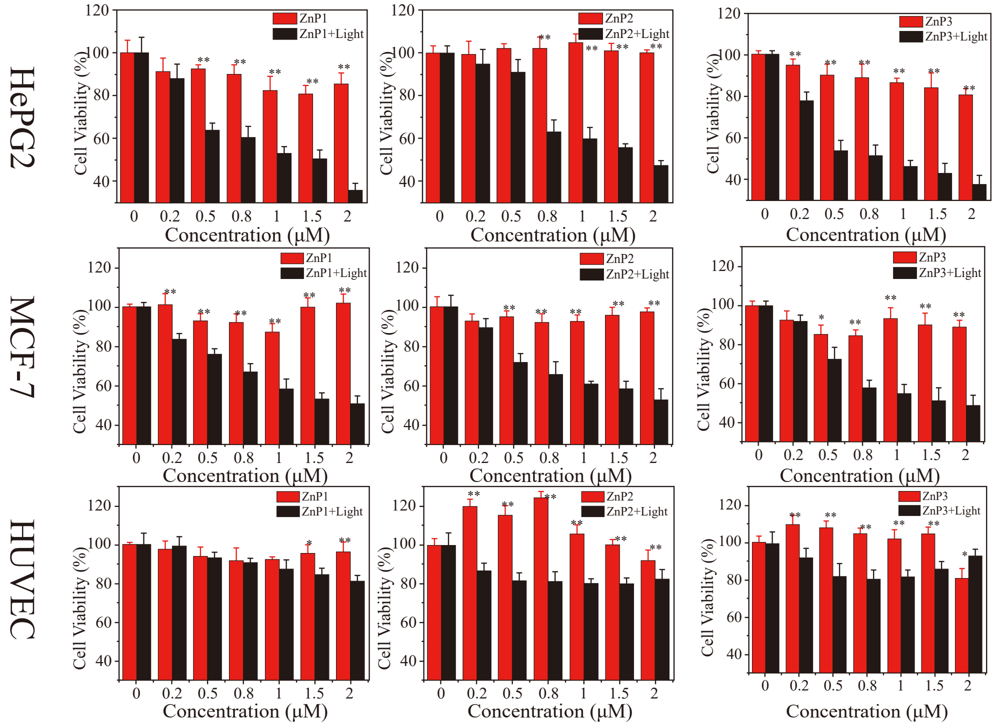

Fig. 4 *In vitro* cytotoxicity of ZnP toward HepG2, MCF-7, and HUVEC cells as determined by the MTT assay. Data are presented as the mean ± SD from three independent experiments ($n = 3$), each performed in technical triplicate. Group comparisons were performed using one-way ANOVA followed by Tukey's post hoc test; * $p < 0.05$, ** $p < 0.01$ vs. control.

investigate the growth inhibition effects of these photosensitizers. The liver, as the primary site of porphyrin metabolism, exhibits high porphyrin accumulation, consistent with physiological principles. Porphyrin derivatives also show elevated uptake in human breast cancer cells. These properties make HepG2 and MCF-7 ideal models for studying porphyrin photosensitizers [33, 35].

Owing to their exceptional phototherapeutic efficacy in cancer treatment and diagnosis, porphyrin nanoparticles have garnered considerable attention in recent years. The 0.2–2.0 μM range was chosen to bracket the anticipated IC_{50}. Pilot studies showed negligible effect below 0.2 μM, whereas dark toxicity emerged at concentrations above 2.0 μM, with cell mortality rising sharply as the upper limit was approached. This window captures the steepest dose-response slope, enabling reliable IC_{50} determination. The range also aligns with clinical photosensitizers (e.g., Photofrin® 1–5 μM) while leveraging enhanced uptake of our porphyrins to achieve efficacy at lower concentrations [8, 36–38].

Under 600–610 nm LED light irradiation, the inhibitory effects of the three PSs on HepG2 cells intensified with increasing photosensitizer concentration, indicating a significant concentration-dependent effect. Conversely, under dark conditions, even at a concentration of 2 μM, the cell viability remained as high as 90%, indicating that ZnP1–ZnP3 exhibit potent inhibitory effects on HepG2 cells (Fig. 4). To further quantify these effects, the IC_{50} values provide a more direct means of comparing the toxicity of ZnP1–ZnP3 toward HepG2 cells. As shown in Table 2, the IC_{50} values of ZnP1–ZnP3 are all below 2 μM under light conditions, with ZnP3 exhibiting a more pronounced cancer cell inhibition rate than ZnP1 and ZnP2. This enhanced efficacy is attributed to the increasing contribution of halogen atoms, as their atomic mass and size increase, leading to higher SOC values [39], which in turn affect the cancer cell inhibition rate. Subsequently, we investigated the inhibitory effects of ZnP1–ZnP3 molecules on MCF-7 cells under uniform experimental conditions, yielding consistent results. Notably, cell viability readings occasionally exceeded 100%. This is a well-known artifact in MTT assays, arising from the temporary enhancement of mitochondrial dehydrogenase activity by porphyrins, which does not reflect genuine cell proliferation [40]. To ensure full transparency, we report the raw, unadjusted values as observed.

In this study, zinc porphyrin derivatives ZnP1–ZnP3 demonstrated significantly higher selective cytotoxicity toward HepG2 and MCF-7 cancer cells compared to normal HUVECs under identical photodynamic conditions. This selectivity can be attributed to three key mechanisms: (1) Enhanced cancer cell

Table 2 IC_{50} values of ZnP1–ZnP3 in HepG2, MCF-7, and HUVEC cells.

Compound	IC_{50} (μM)		
	HepG2	MCF-7	HUVEC
ZnP1	> 2	> 2	> 2
ZnP2	> 2	> 2	> 2
ZnP3	> 2	> 2	> 2
ZnP1+light	1.638	2.011	> 2
ZnP2+light	1.211	1.871	> 2
ZnP3+light	0.875	1.478	> 2

uptake via GRP78/estrogen receptor-mediated endocytosis, while HUVECs rely on passive diffusion [35, 41]; (2) Reduced antioxidant capacity (lower GSH and SOD) in cancer cells, increasing ROS susceptibility [42, 43]; and (3) Acidic tumor microenvironment (pH 6.5–7.0) enhancing uptake of N-alkylated, positively-charged photosensitizers through electrostatic interactions [36–38].

Cell staining and cell cycle

To investigate the phototoxic effects, we utilized staining method with Hoechst 33342 and propidium iodide (PI) and chose HepG2 cells for fluorescence staining experiments to verify the photodynamic toxicity induced by ZnP3.

After 10 min of exposure to 600–610 nm LED light, cells treated with a ZnP3 concentration of 0.5 μM exhibited a significant degree of red fluorescence, and some cells enlarged, indicating cell death or apoptosis. Upon increasing the ZnP3 concentration to 2 μM, the cell nuclei either enlarged or shrank, the blue fluorescence intensified, and the red fluorescence significantly increased, suggesting that apoptosis or cell death occurred following treatment. These findings indicate that ZnP3 induces apoptosis in HepG2 cells under light conditions (Fig. 5), with the effect being dose-dependent.

Conversely, under dark conditions, nearly all cells in the control group exhibited blue fluorescence without any nuclear enlargement or shrinkage, indicating minimal dark toxicity of the photosensitizer and no induction of cell apoptosis or death. The cell cycle arrest data for cells subjected to various conditions are summarized in Fig. S2. The S phase value for ZnP3 increased from 22.77% to 40.11%. Unlike other groups, the S phase was altered under 600–610 nm light. The cell cycle analysis results demonstrate that HepG2 cells are arrested by PSs.

Intracellular ROS detection

To detect the production of reactive oxygen species *in vitro*, we employed DCFH-DA as a ROS probe. Some cells were enlarged. In these cells, esterases cleave the diacetate group of DCFH-DA to form DCFH, which is then oxidized by ROS to the fluorescent compound 2′,7′-dichlorofluorescein (DCF). This compound emits green fluorescence, which can be visualized using a fluorescence microscope [44].

Under light conditions, when the concentration of ZnP3 is 0.5 μM, a degree of green fluorescence emerges in the detected cells. Elevating the concentration of ZnP3 to 2 μM leads to a significant increase in green fluorescence, indicating that photosensitizers are capable of producing reactive oxygen species under illumination. This ROS generation is attributed to the high efficiency of porphyrin compounds in producing singlet oxygen under light conditions, with the quantity of ROS being dose-dependent (Fig. 6).

Conversely, under dark conditions, no green fluorescence is detected at ZnP3 concentrations of 0.5 μM and 2 μM, indicating no ROS production. After entering the cells, DCFH-DA is deacetylated by intracellular esterases and then oxidized by ROS to produce the fluorescent compound 2′,7′-dichlorofluorescein (DCF). This outcome demonstrates that ZnP1–ZnP3 can function as potent sensitizers in the photodynamic therapy process, generating ROS specifically under light irradiation to eliminate cancer cells (Fig. 6).

CONCLUSION

Metallization can modify the electrochemical, spectroscopic, photochemical, and photophysical characteristics of photosensitizers in phototherapy. Moreover, the coordination of zinc with the porphyrin ring reduces hydrophobicity and enhances cellular uptake, thereby augmenting the complex's ability to generate singlet oxygen. Building on these principles, we incorporated zinc into three halogen-containing A2B2 porphyrins and enhanced their aqueous solubility through N-pyridyl-substituted alkylation. Subsequently, we designed and synthesized three zinc-containing complexes (ZnP1–ZnP3). We observed that the growth inhibition rate of the sensitizer on HUVEC cells was lower, regardless of whether it was under light or dark conditions. Consistent with these observations, the IC_{50} value for HUVEC cells was substantially higher than that for cancer cells, indicating that the sensitizer selectively targets cancer cells during the PDT process, with preferential localization around them. Furthermore, due to the heavy atom effect, bromine-containing ZnP3 achieves the highest *in vitro* photocytotoxic efficacy among the three photosensitizers. Therefore, porphyrin photosensitizers offer superior PDT therapeutic effects and hold extensive application potential. This study has several limitations that should be acknowledged. The *in vitro* findings are based on a limited set of cancer cell lines (HepG2 and MCF-7), which may not represent the full heterogeneity of human tumors. The photophysical properties and singlet oxygen yields were characterized in solution (DMSO), which may not fully replicate the tumor microenvironment. Theoretical DFT calculations were

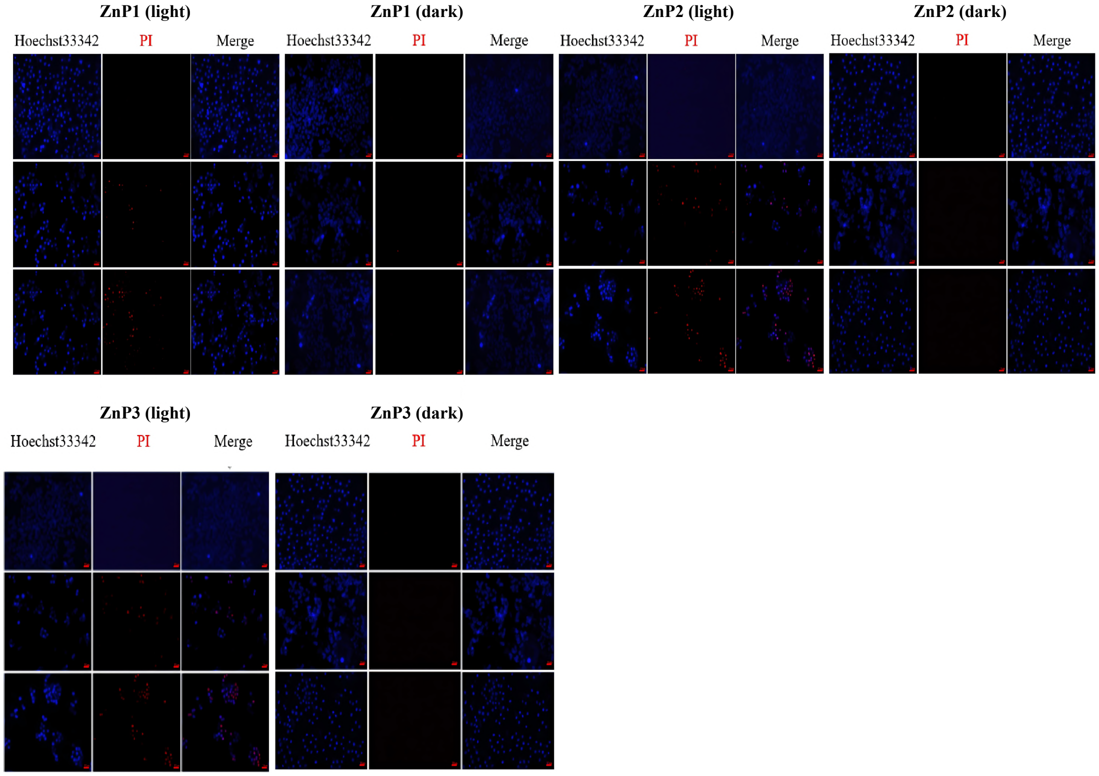

Fig. 5 Hoechst 33342 (live cells and overcoming cells: blue) and PI (dead cells, dying cells, and necrotic cells: red) staining of HepG2 cells treated with different concentrations of ZnP3 under light and dark conditions for 24 h. Fluorescence images are shown. Each group was performed in triplicate.

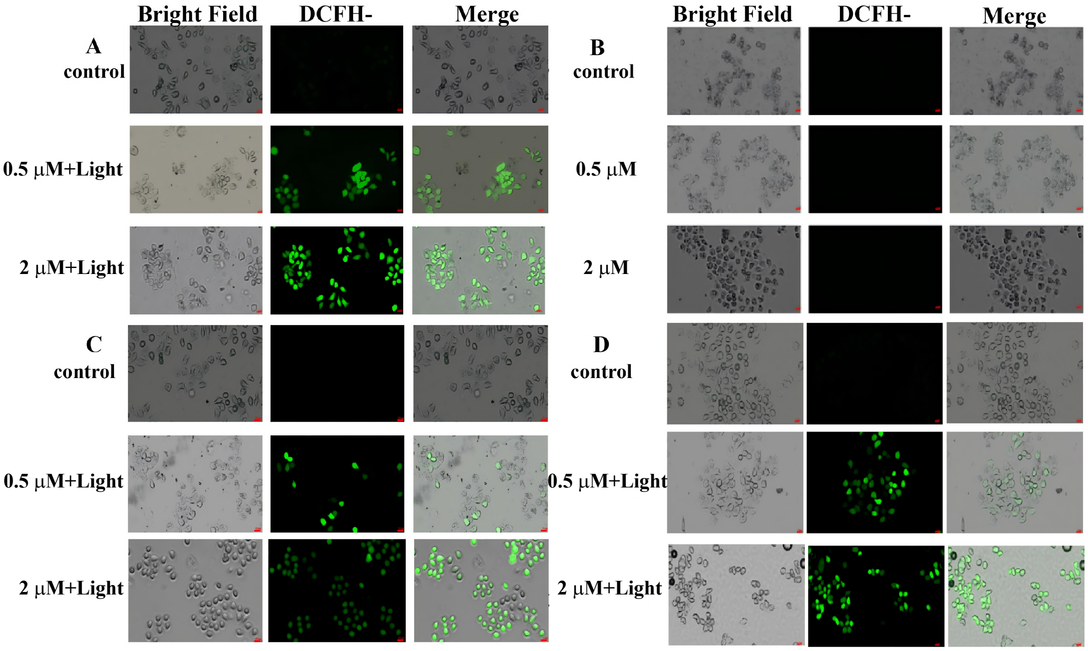

Fig. 6 *In vitro* ROS production by ZnP3 (A–B), ZnP1 (C), and ZnP2 (D) under light irradiation (600–610 nm, 10 min), as indicated by DCF fluorescence. Each group was performed in triplicate.

performed in the gas phase, neglecting solvent effects that could influence electronic properties. These limitations highlight the need for further preclinical investigation to substantiate the translational potential of the ZnP1–ZnP3 photosensitizers. The liver tissue in porphyrin metabolism validates HepG2 as a clinically relevant model for hepatocellular carcinoma, while MCF-7 cells offer an appropriate platform for investigating hormone receptor-driven porphyrin accumulation in breast cancer. This study thereby provides compelling pre-clinical evidence to support the development of halogenated zinc porphyrin photosensitizers for the treatment of both hepatocellular carcinoma and breast cancer.

Appendix A. Supplementary data

Supplementary data associated with this article can be found at https://dx.doi.org/10.2306/scienceasia1513-1874.2026.036.

Acknowledgements: This work was supported by the Major Science and Technology Projects in Gansu Province (No. 22ZD6NA009) and the Research Program sponsored by the State Key Laboratory of Aridland Crop Science of China (No. GSCS2023-Z01). We also thank the support for DFT of Gansu computing Center of China.

REFERENCES

1. Therasse P, Arbuck SG, Eisenhauer EA, Wanders J, Kaplan RS, Rubinstein L, Verweij J, Van Glabbeke M, et al (2000) New guidelines to evaluate the response to treatment in solid tumors. *J Natl Cancer Inst* **92**, 205–216.
2. Twelves C, Wong A, Nowacki MP, Abt M, Burris III H, Carrato A, Cassidy J, Cervantes A, et al (2005) Capecitabine as adjuvant treatment for stage III colon cancer. *N Engl J Med* **352**, 2696–2704.
3. Emoto S, Ishigami H, Yamashita H, Yamaguchi H, Kaisaki S, Kitayama J (2012) Clinical significance of CA125 and CA72-4 in gastric cancer with peritoneal dissemination. *Gastric Cancer* **15**, 154–161.
4. Pérez-Herrero E, Fernández-Medarde A (2015) Advanced targeted therapies in cancer: drug nanocarriers, the future of chemotherapy. *Eur J Pharm Biopharm* **93**, 52–79.
5. Li X, Zheng BD, Peng XH, Li SZ, Ying JW, Zhao Yy, Huang JD, Yoon Jy (2019) Phthalocyanines as medicinal photosensitizers: developments in the last five years. *Coord Chem Rev* **379**, 147–160.
6. Juarranz Á, Jaén P, Sanz-Rodríguez F, Cuevas J, González S (2008) Photodynamic therapy of cancer. Basic principles and applications. *Clin Transl Oncol* **10**, 148–154.
7. Oleinick NL, Morris RL, Belichenko I (2002) The role of apoptosis in response to photodynamic therapy: what, where, why, and how. *Photochem Photobiol Sci* **1**, 1–21.
8. Abo-Zeid MAM, Abo-Elfadl MT, Mostafa SM (2018) Photodynamic therapy using 5-aminolevulinic acid triggered DNA damage of adenocarcinoma breast cancer and hepatocellular carcinoma cell lines. *Photodiagnosis Photodyn Ther* **21**, 351–356.
9. Klyta M, Ostasiewicz P, Jurczyszyn K, Duś K, Latos-Grażyński L, Pacholska-Dudziak E, Ziółkowski P (2011) Vacata- and divacataporphyrin: new photosensitizers for application in photodynamic therapy—an *in vitro* study. *Lasers Surg Med* **43**, 607–613.
10. MacDonald IJ, Morgan J, Bellnier DA, Paszkiewicz GML, Whitaker JE, Litchfield DJ, Dougherty TJ (1999) Subcellular localization patterns and their relationship to photodynamic activity of pyropheophorbide-a derivatives. *Photochem Photobiol* **70**, 789–797.
11. Staneloudi C, Smith KA, Hudson R, Malatesti N, Savoie H, Boyle RW, Greenman J (2007) Development and characterization of novel photosensitizer: scFv conjugates for use in photodynamic therapy of cancer. *Immunology* **120**, 512–517.
12. Kim JY, Choi WI, Kim M, Tae G (2013) Tumor-targeting nanogel that can function independently for both photodynamic and photothermal therapy and its synergy from the procedure of PDT followed by PTT. *J Control Release* **171**, 113–121.
13. Dąbrowski JM, Pucelik B, Pereira MM, Arnaut LG, Stochel G (2015) Towards tuning PDT relevant photosensitizer properties: comparative study for the free and Zn^{2+} coordinated meso-tetrakis [2,6-difluoro-5-(N-methylsulfamylo)phenyl]porphyrin. *J Coord Chem* **68**, 3116–3134.
14. Turan IS, Yildiz D, Turksoy A, Gunaydin G, Akkaya EU (2016) A bifunctional photosensitizer for enhanced fractional photodynamic therapy: singlet oxygen generation in the presence and absence of light. *Angew Chem Int Ed* **55**, 2875–2878.
15. De Simone BC, Mazzone G, Pirillo J, Russoa N, Sicilia E (2017) Halogen atom effect on the photophysical properties of substituted aza-BODIPY derivatives. *Phys Chem Chem Phys* **19**, 2530–2536.
16. Szaciłowski K, Macyk W, Drzewiecka-Matuszek A, Brindell M, Stochel G (2005) Bioinorganic photochemistry: frontiers and mechanisms. *Chem Rev* **105**, 2647–2694.
17. Huang H, Song W, Rieffel J, Lovell JF (2015) Emerging applications of porphyrins in photomedicine. *Front Phys* **3**, 23.
18. Li Yy, Li Gc, Zhang Q, Li Yx, Jia Qf, Zhang Wy, Feng Xx, Xu Wb, et al (2021) Heavy atom effect on water-soluble porphyrin photosensitizers for photodynamic therapy. *Chem Phys Lett* **784**, 139091.
19. Regehly M, Greish K, Rancan F, Maeda H, Böhm F, Röder B (2007) Water-soluble polymer conjugates of ZnPP for photodynamic tumor therapy. *Bioconjug Chem* **18**, 494–499.
20. Youssef TE, Al-Jameel SS, Al-Magribi WM (2020) An effective invasive therapeutic approach of fluoro-substituted zinc phthalocyanine derivatives as potential photosensitizer for prostate carcinoma. *ScienceAsia* **46**, 686–690.
21. Gollavelli G, Ling YC (2014) Magnetic and fluorescent graphene for dual modal imaging and single light induced photothermal and photodynamic therapy of cancer cells. *Biomaterials* **35**, 4499–4507.
22. Turksoy A, Yildiz D, Akkaya EU (2019) Photosensitization and controlled photosensitization with BODIPY dyes. *Coord Chem Rev* **379**, 47–64.
23. Pushpanandan P, Maurya YK, Omagari T, Hirosawa R, Ishida M, Mori S, Yasutake Y, Fukatsu S, et al (2017) Singly and doubly N-confused calix[4]phyrin organoplatinum(II) complexes as near-IR triplet sensi-

tizers. *Inorg Chem* **56**, 12572–12580.

24. Pandey V, Raza MK, Joshi P, Gupta I (2020) Synthesis of water-soluble thioglycosylated trans-A2B2 type porphyrins: cellular uptake studies and photodynamic efficiency. *J Org Chem* **85**, 6309–6322.
25. De Simone BC, Mazzone G, Russo N, Sicilia E, Toscano M (2018) Computational investigation of the influence of halogen atoms on the photophysical properties of tetraphenylporphyrin and its Zinc(II) complexes. *J Phys Chem A* **122**, 2809–2815.
26. Humphrey W, Dalke A, Schulten K (1996) VMD: visual molecular dynamics. *J Mol Graph* **14**, 33–38.
27. Lu T, Chen F (2012) Multiwfn: A multifunctional wavefunction analyzer. *J Comput Chem* **33**, 580–592.
28. Yang Z, Zhang Z, Sun Y, Lei Z, Wang D, Ma H, Tang BZ (2021) Incorporating spin-orbit coupling promoted functional group into an enhanced electron DA system: a useful designing concept for fabricating efficient photosensitizer and imaging-guided photodynamic therapy. *Biomaterials* **275**, 120934.
29. Suda K, Yokogawa D (2022) Spin-orbit coupling calculation combined with the reference interaction site model self-consistent field explicitly including constrained spatial electron density distribution. *J Chem Theory Comput* **18**, 6043–6051.
30. Neto DHC, Gotico P, Tran TT, Szantai C, Halime Z, Sircoglou M, Soto J, Steenkeste K, et al (2024) Tracking photoinduced charge separation in a perfluorinated Zn-tetraphenylporphyrin sensitizer. *New J Chem* **48**, 14896–14903.
31. Gust D, Moore TA, Moore AL (2001) Mimicking photosynthetic solar energy transduction. *Acc Chem Res* **34**, 40–48.
32. Imahori H, Sakata Y (1997) Donor-linked fullerenes: photoinduced electron transfer and its potential application. *Adv Mater* **9**, 537–546.
33. Ievtukhov V, Prlj A, Ciupak O, Mońkaa M, Serdiuk IE (2025) Pursuing the holy grail of thermally activated delayed fluorescence emitters: a molecular strategy for reducing the energy gap and enhancing spin-orbit coupling. *Chem Sci* **16**, 11398–11412.
34. Ponte F, Mazzone G, Russo N, Sicilia E (2018) BODIPY for photodynamic therapy applications: computational study of the effect of bromine substitution on 1O2 photosensitization. *J Mol Model* **24**, 183.
35. Harris IS, Treloar AE, Inoue S, Sasaki M, Gorrini C, Lee KC, Yung KY, Brenner D, et al (2015) Glutathione and thioredoxin antioxidant pathways synergize to drive cancer initiation and progression. *Cancer Cell* **27**, 211–222.
36. Zohuri B (2025) Photodynamic therapy (PDT) mathematical and physical principles underlying photodynamic therapy a precision approach to skin treatment. *Japan J Clin Med Res* **5**, 1–3.
37. Wang X, Xia L, Cheng H, Li K, Feng W, Dai X, Chen Y (2024) Ultrasound-mediated Cu^{2+}/Cu^{+} redox cycling activates peroxymonosulfate for oxygen-independent reactive X species (X=O/S) therapy. *Nano Today* **55**, 102180.
38. Kozlova E, Sergunova V, Sherstyukova E, Grechko A, Lyapunova S, Inozemtsev V, Kozlov A, Gudkova O, et al (2023) Mechanochemical synergism of reactive oxygen species influences on RBC membrane. *Int J Mol Sci* **24**, 5952.
39. Alberto ME, De Simone BC, Mazzone G, Siciliab E, Russo N (2015) The heavy atom effect on Zn(II) phthalocyanine derivatives: A theoretical exploration of the photophysical properties. *Phys Chem Chem Phys* **17**, 23595–23601.
40. Berridge MV, Herst PM, Tan AS (2005) Tetrazolium dyes as tools in cell biology: New insights into their cellular reduction. *Biotechnol Annu Rev* **11**, 127–152.
41. Battogtokh G, Gotov O, Subrahmanyam N, Ko YT, Ghandehari H (2019) GRP78-targeted HPMA copolymer-photosensitizer conjugate for hyperthermia-induced enhanced uptake and cytotoxicity in MCF-7 breast cancer cells. *Macromol Biosci* **19**, 1900032.
42. Scholz M, Petusseau AF, Gunn JR, Chapman MS, Pogue BW (2020) Imaging of hypoxia, oxygen consumption and recovery *in vivo* during ALA-photodynamic therapy using delayed fluorescence of protoporphyrin IX. *Photodiagnosis Photodyn Ther* **30**, 101790.
43. Luk K, Zhao IS, Yin IX, Niu JY, Gutknecht N, Chu CH (2021) Irradiation methods of 10,600 nm carbon dioxide laser for dental caries prevention. *Lasers Dent Sci* **5**, 1–8.
44. Rapozzi V, Umezawa K, Xodo LE (2011) Role of NF-κB/Snail/RKIP loop in the response of tumor cells to photodynamic therapy. *Lasers Surg Med* **43**, 575–585.

Appendix A. Supplementary data

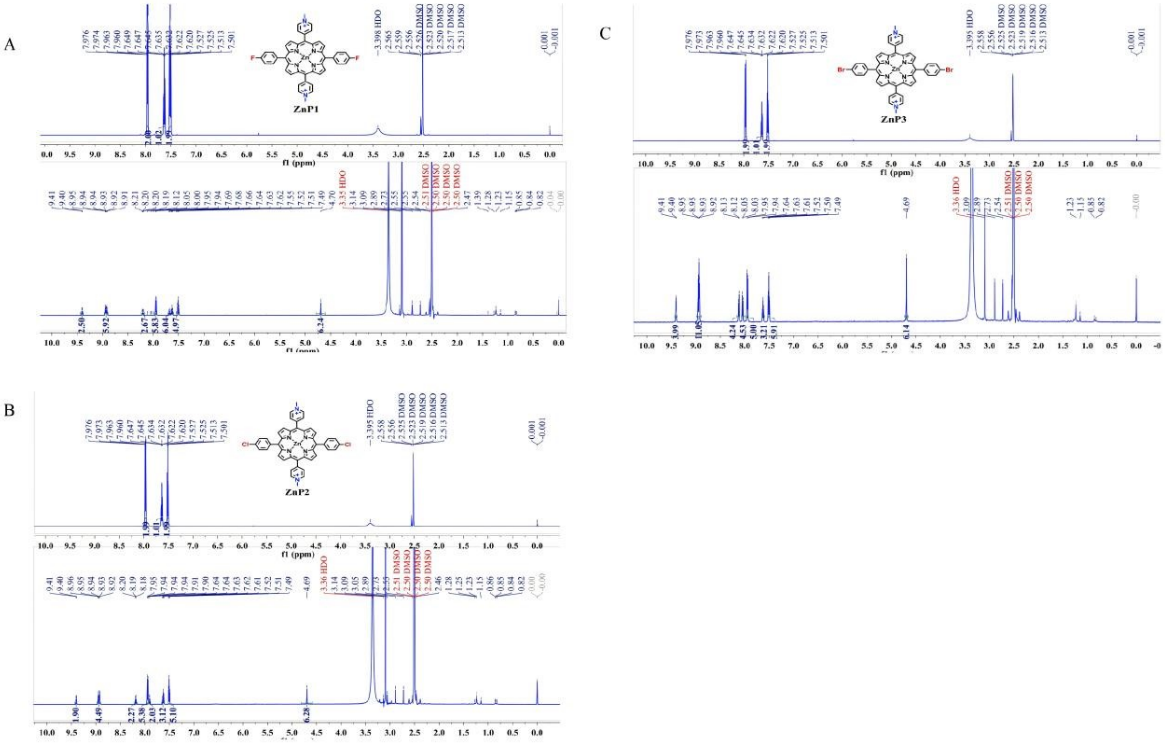

Fig. S1 The ^{1}H-qNMR spectra of ZnP1 (A), ZnP2 (B), and ZnP3 (C), obtained at 600 MHz in DMSO-d_6. The quantitative signals were observed at chemical shift of δ4.70 ppm and δ7.50–7.52 ppm. The purity yields of each compound were 89.64%, 87.02, and 90.63%, respectively.

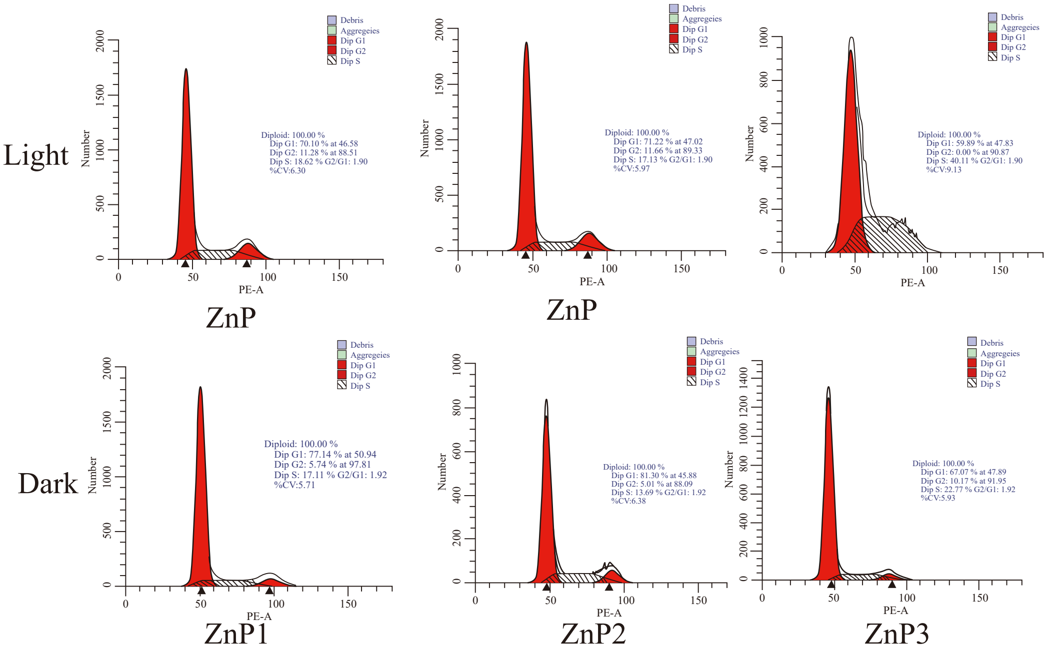

Fig. S2 Cell cycle analysis of HepG2 cells under different conditions.